

Doppler-free spectroscopy and collisional studies with tunable diode lasers of lithium isotopes in a heat-pipe oven

I. E. Olivares and A. E. Duarte

Departamento de Física, Comisión Chilena de Energía Nuclear, Amunategui 95, Santiago, Chile

T. Lokajczyk

Institut für Experimentalphysik V, Ruhr-Universität Bochum, D-44780 Bochum, Germany

A. Dinklage

Institut für Physik, E.-M.-Arndt Universität, Domstrasse 10 a, D-17489 Greifswald, Germany

F. J. Duarte

Eastman Kodak Company, Rochester, New York 14652-3703

Received August 28, 1997; revised manuscript received March 12, 1998

The spectra of the $2s-2p$ lithium transitions were studied in an atomic-lithium vapor-argon-gas mixture by a Doppler-free saturation amplitude modulation spectroscopy technique that employs a tunable diode laser. Lamb-dip and crossover signals were highly resolved. The experimental Doppler-free spectra were used in conjunction with a density matrix method to yield parameters of spectroscopic interest. These parameters include line broadening and relaxation rates that are due to collisions between isotopic species and argon atoms. In addition, Doppler-limited spectra were used to determine density, concentration, and temperature of the lithium isotopes. © 1998 Optical Society of America [S0740-3224(98)02707-6]

OCIS codes: 020.2070, 020.3690, 300.1030, 300.6260, 300.6380, 300.6420.

1. INTRODUCTION

In recent years there has been considerable interest in lithium spectroscopy.¹⁻⁸ Studies of Li isotopes by dye-laser-based Doppler-free spectroscopy have been published.^{7,8} The availability of semiconductor lasers has considerably facilitated experiments in the field of atomic laser spectroscopy because such lasers offer stable narrow-linewidth emission, excellent tunability, and compactness.⁹⁻¹² Specifically, today's diode lasers have linewidths 1000 times smaller than the Doppler width of atomic transitions. Also, diode lasers are stable in the frequency and power domains and can be tuned by electrical, thermal, and optical means.^{11,12} Additionally, because of their compactness and reliability they can substitute for more-complicated coherent sources, such as ring dye lasers, especially in applications that require relatively low power.

We have recorded and studied Doppler-free and Doppler-limited spectra of Li isotopes by using diode-laser-based instrumentation. The diode-laser-generated spectra were recorded as a function of Li density, argon pressure, and laser intensity. In particular, we recorded the Doppler-free spectra of the ${}^6\text{Li } D_2$ line and resolved its hyperfine structure. We chose this transition of ${}^6\text{Li}$ for study because of the apparent lack of published mate-

rial on its characteristics and because it represents an intermediate case of difficulty for our experimental facility.

To describe the dynamics of atomic excitation under the influence of radiation and collisional processes in the case of narrow laser linewidth and high spectral intensity it is necessary to use the density matrix formalism.^{13,14} We have developed a density matrix approach to describe the Doppler-free and Doppler-limited spectra of Li. The theory is used in conjunction with a numerical method that considers all the sublevels of the hyperfine structure of the Li $2s-2p$ transition and the optical pumping and relaxation processes. The hyperfine structure of the ${}^6\text{Li } D_2$ line recorded experimentally was successfully matched theoretically by our density matrix approach. We describe the excitation-relaxation dynamics for the special case of ${}^6\text{Li}$ and derive the parameters of experimental interest such as density, concentration, temperature, line broadening, and relaxation rates that result from velocity-changing collisions.

2. THEORY

From the Wigner-Eckart theorem,¹⁵ and decoupling the J from the I and the L from the S , we arrive at the matrix element for the dipolar electric moment D :

$$\begin{aligned}
|\langle i|D_q|f\rangle|^2 &= |\langle \alpha_i J_i I F_i m_i | D_q | \alpha_f J_f I F_f m_f \rangle|^2 \\
&= \frac{1}{3} C(F_i F_f m_i, -m_f; 1q)^2 (2F_i + 1) \\
&\quad \times (2F_f + 1) W(J_i I 1 F_f; F_i J_f)^2 \delta_{S_i, S_f} \\
&\quad \times (2J_i + 1)(2J_f + 1) \\
&\quad \times W(L_i S_i 1 J_f; J_i L_f)^2 \|D\|^2, \quad (1)
\end{aligned}$$

where m is the quantum number for the axial angular momentum, F is the quantum number for the total angular momentum, I is the nuclear spin quantum number, J is the quantum number for the electronic angular momentum, and α represents the remaining quantum numbers (including the orbital angular momentum L and the electron spin S). Also, i and f are ground and excited levels, respectively, $q = 1$ for transitions that are due to right circularly polarized light, $q = 0$ for plane-polarized light, and $q = -1$ for left circularly polarized light. Here $\|D\| = |\langle \alpha_i \| D \| \alpha_f \rangle|$ is the usual reduced dipole matrix element.

The coefficient for spontaneous emission from state $|f\rangle$ to state $|i\rangle$ is¹⁵

$$a_{fi} = \frac{4\omega^3 K_e}{3\hbar c^3} \sum_q |\langle i|D_q|f\rangle|^2, \quad (2)$$

and the coefficient for spontaneous emission from state $|f\rangle$ to all the states inside a level (n, L_i) is

$$\gamma = \tau^{-1} = A_f = \sum_i a_{fi} = \frac{4\omega^3 K_e}{3\hbar c^3 (2L_f + 1)} \|D\|^2. \quad (3)$$

Thus we can calculate $\|D\|^2$ from Eq. (3), knowing that $\tau = 27.29$ ns (Ref. 16) for the transition $L_f = 1 \rightarrow L_i = 0$ (with $n = 2$) in ${}^6\text{Li}$. Therefore $\|D\|^2 = 1.77 \times 10^{57}$ C²m². The Rabi frequency for each transition for plane-polarized light is given by

$$|\Omega_{if}|^2 = \frac{8\pi I K_e}{c\hbar^2} |\langle i|D_0|f\rangle|^2, \quad (4)$$

where $K_e = 8.99 \times 10^9$ Vm/C and I is the intensity of the laser radiation.

The frequency of each hyperfine structure level is given by Arimondo *et al.*¹⁷ The behavior of atomic populations in the presence of an electromagnetic field is described by the optical Bloch equations obtained from the Liouville equation that considers the atomic Hamiltonian with an interaction term that describes the interaction between the field and the atom. To obtain these equations we use the rotating-wave approximation,¹⁴ the dipolar approximation, and classical theory to describe the electromagnetic field (neglecting the magnetic component). The coherences in the density matrix between ground states or between excited states are negligible if the energetic separation between states is large compared with the natural linewidth and if the saturation parameter $S_0 \ll 1$ or if the homogeneous linewidth is large compared with the natural linewidth.¹³ The other coherences are approximated by stationary states (Wilcox–Lamb approximation).¹⁸ Using these approximations, we have the following expressions for the diagonal matrix elements^{13,19–21}:

$$\begin{aligned}
\dot{\rho}_{ii} &= \sum_f W_{if}(\rho_{ff} - \rho_{ii}) + (\gamma_T + \gamma_{vc})(\rho_{ii}^0 - \rho_{ii}) \\
&\quad + \sum_f a_{fi} \rho_{ff},
\end{aligned}$$

$$\begin{aligned}
\dot{\rho}_{ff} &= \sum_i W_{if}(\rho_{ii} - \rho_{ff}) + (\gamma_T + \gamma_{vc})(\rho_{ff}^0 - \rho_{ff}) - \gamma \rho_{ff}, \quad (5)
\end{aligned}$$

where γ_T is the relaxation rate that is due to the transit time of the atoms in the irradiation zone,²² γ_{vc} is the relaxation rate for velocity-changing collisions^{8,23} (VCC's), and ρ_{ii}^0 is the population of state $|i\rangle$ outside the irradiation zone.

The transition rate is given by

$$W_{if} = \frac{\frac{1}{2} |\Omega_{if}|^2 \Gamma}{(\delta_{if} - kv)^2 + \Gamma^2}, \quad (6)$$

where $\Gamma = \gamma/2 + \Gamma_c + \Gamma_L + \Gamma_T$ is the homogeneous broadening, $\delta_{if} = \omega - \omega_{if}$ is the laser detuning from resonance, $\omega_{if} = 2\pi(\nu_f - \nu_i)$, $\gamma/2$ is the natural linewidth, Γ_c is the broadening that is due to collisions,²² Γ_L is the laser linewidth, and Γ_T is the transit-time broadening.²² Here, ω_{if} is the resonance angular frequency of the line. The apparent pumping by transit among different states is caused by the exit or entrance of atoms in the excitation region. This effect occurs because outside the excitation region the atoms are distributed uniformly among their ground states and inside the region the distribution of levels is controlled by the laser.

The transit-time relaxation rate is given by

$$\gamma_T = v/d, \quad (7)$$

where v is the mean velocity of the atoms and d in this case is the diameter of the laser beam. Transit-time relaxation has been treated in more detail by Gibble and Gallagher.²³

The VCC's act in a way similar to transit-time broadening. VCC's caused by buffer-gas perturbers remove atoms from a velocity group out of resonance and bring atoms from other velocity groups into resonance. When the optical pumping or the buffer-gas pressure is low, the population of the atoms outside the resonant velocity group can be approximated by ρ_{ss}^0 , where s denotes any state. When the collisional relaxation and the spontaneous emission are fast enough with respect to the velocity of the atoms, $\rho_{ff}^0 \approx 0$ and $\rho_{ii}^0 \approx 1/n$, where n is the number of ground states. In the D_2 line of ${}^6\text{Li}$ there are 18 states, grouped into five Zeeman multiplets.

In the experiments presented here we observed that the relaxation is relatively strong. So we can consider the population of each state to be approximately equal to that of the other states of the same multiplet, which permits us to work with only five matrix elements, each representing a complete multiplet as one state. This approximation can be made because the collisional relaxation distributes the population equally among the different substates, and the radiative processes affect the different substates of a single Zeeman multiplet in a similar way.

With these approximations we obtain the equations for all the multiplets included in the numbering of Fig. 1:

$$\begin{aligned}
 \dot{\rho}_{11} &= W_{13}(\rho_{33} - \rho_{11}) + W_{14}(1/2\rho_{44} - \rho_{11}) \\
 &\quad + \gamma(8/9\rho_{33} + 5/9\rho_{44}) + (\gamma_T + \gamma_{vc})(1/3 - \rho_{11}), \\
 \dot{\rho}_{22} &= W_{25}(2/3\rho_{55} - \rho_{22}) + W_{24}(\rho_{44} - \rho_{22}) \\
 &\quad + W_{23}(\rho_{33} - 1/2\rho_{22}) + \gamma(1/9\rho_{33} + 4/9\rho_{44} + \rho_{55}) \\
 &\quad + (\gamma_T + \gamma_{vc})(2/3 - \rho_{22}), \\
 \dot{\rho}_{33} &= W_{13}(\rho_{11} - \rho_{33}) + W_{23}(1/2\rho_{22} - \rho_{33}) - \gamma\rho_{33} \\
 &\quad - (\gamma_T + \gamma_{vc})\rho_{33}, \\
 \dot{\rho}_{44} &= W_{24}(\rho_{22} - \rho_{44}) + W_{14}(\rho_{11} - 1/2\rho_{44}) - \gamma\rho_{44} \\
 &\quad - (\gamma_T + \gamma_{vc})\rho_{44}; \\
 1 &= \rho_{11} + \rho_{22} + \rho_{33} + \rho_{44} + \rho_{55}.
 \end{aligned}
 \tag{8}$$

The subscripts 1 and 2 denote the $F = 1/2$ and $F = 3/2$ components of the $2s$ level; the subscripts 3, 4, 5, and the $F = 1/2$, $F = 3/2$, and $F = 5/2$ components of the $2p \ ^2P_{3/2}$ state, respectively. ρ_{kk} for a given multiplet k is the sum of the populations of the sublevels of the multiplet k . W_{jk} for a transition between multiplets j and k

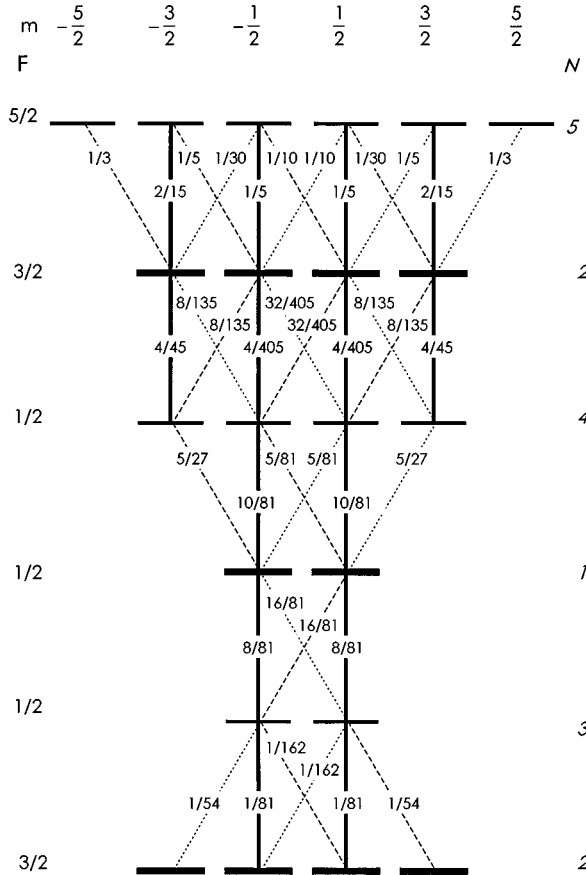


Fig. 1. Values of $N_{ifq} = |\langle i|D_q|f\rangle|^2/|D|^2$ for each transition of Li. N labels the five Zeeman multiplets discussed in the text (note that $N = 2$ is shown twice). Thicker horizontal lines, ground states ($J = 1/2$); thinner horizontal lines, excited states ($J = 3/2$); dotted lines, transitions with $q = -1$; vertical lines, transitions with $q = 0$; dashed lines, transitions with $q = 1$.

is the average of W_{ij} for transitions among the sublevels of the multiplets j and k . Other relaxation rates that are due to electron randomization²⁴ are neglected because they are 8 orders of magnitude smaller than the relaxation caused by the VCC's. The cross section for VCC is $\sigma_{vc} \approx 10^{-14} \text{ cm}^2$,⁸ and σ for electron randomization is approximately 10^{-22} cm^2 .²⁴ The resonance energy transfer cross section for the $^7\text{Li}(2P) - ^6\text{Li}(2P)$ process, σ_{tr} ,² and σ_{vc} are both of the order of 10^{-14} cm^2 . However, $\gamma_{vc} \gg \gamma_{tr}$, where γ_{tr} is the excitation transfer relaxation rate, because $\gamma_{vc} = \sigma_{vc} v n_{Ar}$ (v is the Li-Ar relative velocity and n_{Ar} is the Ar density) and $\gamma_{tr} = \sigma_{tr} v n_{Li}$ (v is the Li-Li relative velocity and n_{Li} is the lithium density). In our experiments $n_{Ar} \approx 10^{16} \text{ cm}^{-3}$ and $n_{Li} \approx 5 \times 10^9 \text{ cm}^{-3}$; thus we can neglect the excitation transfer mechanisms. For the broadening mechanisms that are due to other relaxation processes, similar arguments apply: Because the spectral line broadening is of the same order as the relaxation rate of the associated transition,²² we have that the broadening of the Li spectral line owing to collisions of the Li with the Ar atoms is much larger than self-broadening (Li-Li collisions). For the density mentioned above we can neglect radiation trapping, according to the Holstein theory.²⁵

The atomic absorption coefficient is obtained from the imaginary part of the susceptibility, which is related to the macroscopic polarization of the gas, and the polarization is obtained from the density matrix as the mean value of the dipole operator.¹⁴ Thus the absorption of the laser light in a vapor with density n and length dx , according to Eqs. (5), is given by

$$dI = h \nu_{if} n \left\langle \sum_{if} W_{if} (\rho_{ff} - \rho_{ii}) \right\rangle dx = -h \nu_{if} n \gamma' \langle \rho_e \rangle dx,
 \tag{10}$$

where the angle brackets indicate the average over the velocity distribution for vapor at temperature T , given by

$$F(v) = \left(\frac{m}{2\pi k_B T} \right)^{1/2} \exp\left(-\frac{mv^2}{2k_B T} \right),
 \tag{11}$$

and $\gamma' = \gamma + \gamma_T + \gamma_{vc}$ and $\rho_e = \rho_{33} + \rho_{44} + \rho_{55}$ is the total population for the various excited states.

Extending the absorption equations to the Doppler-free saturation spectroscopy amplitude modulation case, we have

$$\begin{aligned}
 dI_d^0 - dI_d &= h \nu_{if} n \left\langle \sum_{if} W_{if}^+ (\rho_{ff}^+ - \rho_{ii}^+) \right\rangle dx \\
 &\quad - h \nu_{if} n \left\langle \sum_{if} W_{if}^+ (\rho_{ff}^- - \rho_{ii}^-) \right\rangle dx,
 \end{aligned}
 \tag{12}$$

where the population depends on $W^+ = W(I_d, v)$, which is the transition rate given by the diagnostic beam (with intensity I_d) and $W^- = W(I_p, -v)$, which is the transition rate given by the pump beam (with intensity I_p) propagating in the opposite direction. $\rho_{ii}^+ = \rho_{ii}(W^+)$, $\rho_{ii}^- = \rho_{ii}(W^+ + W^-)$, dI_d^0 is the absorption during the dark periods of the modulation cycle ($I_p = 0$), and dI_d is the absorption during the illumination period.

Inasmuch as the spectra were obtained with high transmittance, dI_d^0 and dI_d are nearly independent of x , and the transmittance is approximately linear with dI/dx , then the amplitude of the spectrum is nearly proportional to $(dI_d^0 - dI_d)/dx$ and the spectral line can be described by Eq. (12).

Equations (8) were solved numerically for ρ_{ii} in the steady state. The results were inserted into Eq. (12), and the mean values were calculated by Simpson's rule. Equation (12) was fitted to each experimental spectrum. The fit parameters were γ_{vc} and Γ . The temperature and the intensity were constants. We used the Marquardt fitting method²⁶; γ_T should be calculated with Eq. (7).

The Doppler-free spectra were scanned for some values of intensity and pressures, and the results of the fitting were extrapolated to $I_p = 0$, where the approximations made are optimal (coherences neglected and signal proportional to dI/dx). In this case the absolute value of I_p is not relevant. The values of Γ and γ_{vc} obtained at $I_p = 0$ are the results discussed in Section 4 below.

For sufficiently strong collisional relaxation we can assume that all the ground substrates have an equal population, which is also valid for the excited states. When the optical pumping rate is slow compared with the collisional transition rate we can make the two-state approximation. Then Eqs. (8) reduce to

$$\dot{\rho}_g = W_{ge} \left(\frac{g_g}{g_e} \rho_e - \rho_g \right) + \gamma' \rho_e, \quad (13)$$

where $\rho_g = \rho_{11} + \rho_{22}$ is the population of the ground states, $\rho_{11} = \rho_g/3$, $\rho_{22} = 2\rho_g/3$, $\rho_{33} = \rho_e/6$, $\rho_{44} = \rho_e/3$, and $\rho_{55} = \rho_e/2$. The transition rate W_{ge} is the sum of the transition rates W_{ij} divided by the number of ground states, and g_e and g_g are the degeneracies of each level. Considering Eq. (10),

$$dI = -\sigma I n dx, \quad (14)$$

and because the homogeneous broadening is small compared with the Doppler width, we have that the absorption cross section is given by

$$\sigma = \frac{h\nu\gamma'}{I} \langle \rho_e \rangle \approx \frac{h\nu\gamma'}{I} \int F(\delta/k) \rho_e(\delta = 0) d\nu. \quad (15)$$

Isolating ρ_e in the steady state [from Eq. (13)] and inserting it into relation (15), we obtain the absorption coefficient

$$k_\nu = \sigma n = \frac{g_e n \lambda^2 \sqrt{\ln 2}}{g_g \tau} \frac{1}{4\pi^{3/2}} \frac{1}{\Delta\nu_D} \frac{1}{\sqrt{1+S_0}} \times \exp\left[-\frac{4\ln 2}{\Delta\nu_D^2} (\nu - \nu_0)^2\right], \quad (16)$$

where

$$\Delta\nu_D = \left(\frac{8k_B T \ln 2}{m\lambda^2} \right)^{1/2} \quad (17)$$

is the Doppler width and

$$S_0 = \frac{1}{2} \left(1 + \frac{g_g}{g_e} \right) \frac{1}{\gamma'\Gamma} \frac{\lambda^3 I}{2\pi c h \tau} \frac{g_e}{g_g} \quad (18)$$

is the saturation parameter. In the Doppler-limited experiment $I = 1.4 \mu\text{W}$ in 1 mm^2 and $S_0 = 0.001$. We can neglect S_0 in Eq. (16).

The intensity of the transmitted light is given according to Eq. (14) by

$$I_\nu = I_0 \exp(-k_\nu x), \quad (19)$$

where k_ν is the absorption coefficient and x is the length of the Li-vapor path. I_ν and I_0 are the transmitted and the incident intensity, respectively, at a given frequency. From these intensities the background light has to be subtracted.

The density, concentration, and temperature of the Li isotopes are the fitted parameters that we obtained by fitting Eq. (19) with k_ν given by Eq. (16) to the experimental transmittance value I_ν/I_0 , using a MathLab code that uses a Simplex procedure.

The density n of the different isotopes can also be obtained by use of the integral of the absorption coefficient k_ν over each line, which yields

$$\int k_\nu d\nu = \frac{\lambda_0^2 g_e n}{8\pi g_g \tau}. \quad (20)$$

The temperature can also be estimated from Eq. (17).

3. EXPERIMENT

We measured Doppler-limited lines for the $2s-2p$ absorption in an Ar-embedded stationary Li vapor produced in a heat-pipe cell (Comstock Model HP-802).

The heat-pipe technology was described previously.^{27,28} This cell permits the heating of Li to 700 °C. The cell should be purged initially and be held at a pressure of 2–3 Torr of Ar, which is used as a buffer gas to avoid deposition of Li onto the windows. The cell includes a Li collection system for reutilization of the Li condensed in the cold regions. The main feature of the heat-pipe oven is that it allows one to obtain an isothermal vapor with constant density and clean windows for absorption measurements.

For excitation with narrow-band laser emission we used a cw external-cavity tunable diode laser (NewFocus Model 6200) with a central wavelength of 671 nm, tunable over 12 nm with a power of 6 mW. It has a line-width of <5 MHz and a wavelength stability of <0.01 nm/day. The cavity uses a grazing-incidence configuration.¹¹ The design of the laser cavity includes an external grating that acts as a narrow spectral filter and forces the laser to operate in a single longitudinal mode. We can fine tune the wavelengths by changing the grating angle with a piezoelectric transducer. The center wavelength can also be achieved by control of current, temperature, or both and by picometer setting of the diode laser.

Unwanted background radiation is produced by laboratory light and the side modes of the diode laser. The side mode suppression is ~40 dB, and we measured a 3% background compared with that of the unabsorbed signal. We subtracted the background for all the spectra.

The laser beam was aligned through the Li vapor and detected by a photodiode (EG&G Model FND100) and a

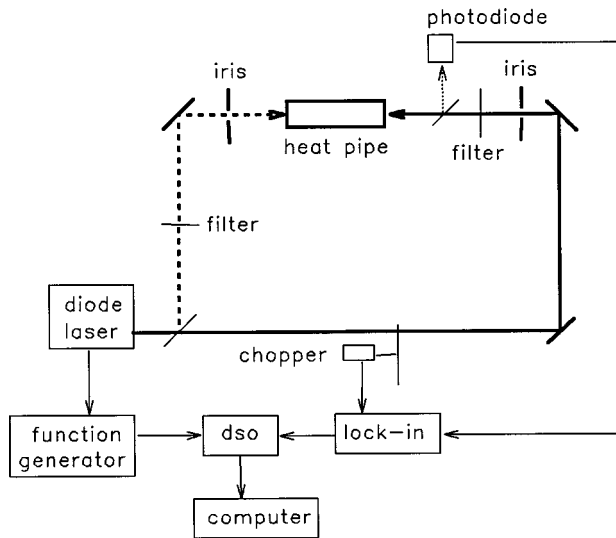


Fig. 2. Doppler-free experimental setup: dso, digital storage oscilloscope.

400-MHz digital storage oscilloscope (LeCroy Model 9310A). We scanned the spectra by rotating the grating.

We measured the wavelengths with a wavemeter (Burleigh Instruments Model WA-4500). The saturation intensity for the ${}^6\text{Li } D_2$ line is obtained when $S_0 = 1$, and in our experiments $\Gamma = 5 \times 10^7 \text{ s}^{-1}$ and $I_s = 206 \text{ W/m}^2$.

Based on the fact that the diode laser used in our experiment has a high spectral intensity, we also performed saturation spectroscopy studies. In particular, we followed up techniques previously proposed.²² Figure 2 depicts the experimental setup. We scanned the Doppler-free spectra with the diode laser over the D_2 line of ${}^6\text{Li}$ in the heat-pipe oven with the modulated amplitude technique, using a lock-in amplifier (Standard Research Systems Model SR510). In the Doppler-limited experiment the lock-in technique was not used.

For all experiments we used 95% enriched ${}^6\text{Li}$. We experimentally removed the broad background of the Doppler-limited profile by using the lock-in technique. The spectra were measured for different Ar pressures and different values for the pump beam I_p . To scan the spectra we used a function generator. We also employed a low scanning frequency (0.1 Hz) to maximize the resolution and to minimize the RC distortion and the noise of the spectra. The heat-pipe oven was kept at a low enough temperature (375 °C) to yield high transmittance (≈ 0.8) and low density ($n = 5 \times 10^9 \text{ cm}^{-3}$), which minimize the effect of radiation trapping and simplify the calculation by producing relatively constant values of I along the heat-pipe oven. Pump intensity I_p was modulated with a chopper at 1046 Hz. With lower frequencies the noise increases, and at high frequencies the populations do not reach steady state during every cycle. The probe beam intensity I_d was 0.8 W/m^2 . It is convenient to use a low probe intensity to minimize the broadening and the dependence of the spectra on I_d that can be detected with the photodiode without causing its saturation. In this case the intensity I_p should be high enough to be above the noise level. The lock-in amplifier was used with time constants low enough to avoid RC distortion but high

enough to avoid excessive noise. The laser beam was directed into the heat-pipe oven through a 2-mm circular aperture. The power was measured with a powermeter (Newport Model 1815C/818SL) at the exit of the apertures.

4. RESULTS AND DISCUSSION

Typical Doppler-limited absorption spectra are shown in Fig. 3(a). In addition, spectra of the further cases involving large optical depth are also of interest and are shown in Fig. 3(b). The circles in these figures represent experimental points, and the curves are theoretical fits from Eqs. (16) and (19). In Fig. 4 we plot the pressure obtained from the absorption results of density and temperature and the ideal gas law as a function of temperature for the two Li isotopes. These values were obtained experimentally; the solid curve is the vapor-pressure curve for natural Li from the CRC tables.²⁹ The discrepancy between the measured vapor-pressure curves obtained from the absorption experiments and from the CRC tables arises because the temperature is measured

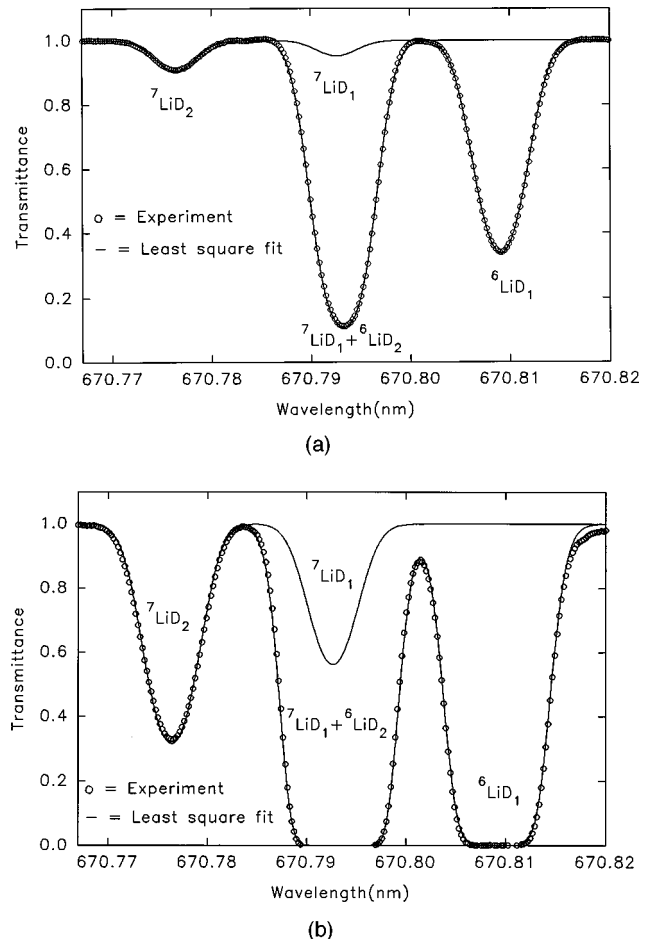


Fig. 3. (a) Doppler-limited Li lines. Experimental and least-squares fits for ${}^7\text{Li}$ only and for the sum of ${}^6\text{Li}$ and ${}^7\text{Li}$. $n({}^7\text{Li}) = 1.9 \times 10^9 \text{ cm}^{-3}$, $n({}^6\text{Li}) = 4.6 \times 10^{10} \text{ cm}^{-3}$, $T = 408 \text{ }^\circ\text{C}$, ${}^7\text{Li}(4.1\%)$. (b) Optically thick Doppler-limited Li lines. Experimental and least-squares fits for ${}^7\text{Li}$ only and for the sum of ${}^6\text{Li}$ and ${}^7\text{Li}$. $n({}^7\text{Li}) = 2.5 \times 10^{10} \text{ cm}^{-3}$, $n({}^6\text{Li}) = 4.3 \times 10^{11} \text{ cm}^{-3}$, $T = 549 \text{ }^\circ\text{C}$.

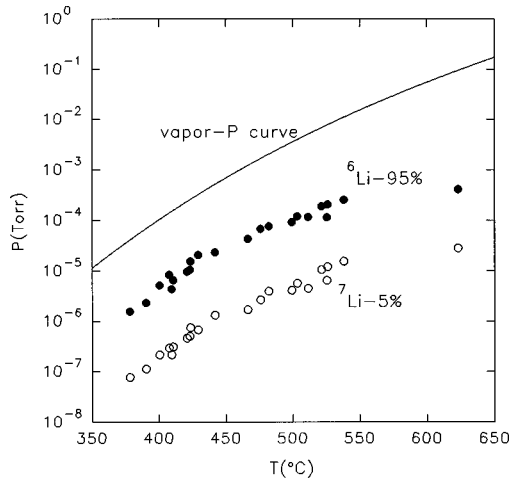


Fig. 4. Vapor-pressure curves for ${}^6\text{Li}$ and ${}^7\text{Li}$. The solid curve was obtained from the literature.²⁹ Circles, experimental data: T and n were obtained from fitting of the Doppler-limited absorption spectra and P from the ideal gas law.

optically (by use of the Doppler-limited spectra) along the heat-pipe oven axis where it is higher than the average temperature of the vapor considered in the CRC tables. This result is due to the large heat transfer between the evaporation zone and the condensation zone, which leads to significant vapor-flow velocities along the axis of the heat-pipe oven.²⁷

A typical Doppler-free spectrum for the ${}^6\text{Li}$ D_2 line at low Ar pressure is shown in Fig. 5(a). We can observe a crossover signal in this figure at the center of the trace caused by double resonance. The right and left peak lines correspond to the transitions $2s(F=1/2)-2p$ and $2s(F=3/2)-2p$ hyperfine lines, respectively, separated by 228 MHz.^{7,17} This experimental spectrum shows excellent resolution of the hyperfine structure and is fairly well fitted by our density matrix model: This is the main result of this study. The negative crossover signal is caused when the probe beam is tuned to one of the two transitions of the D_2 line with a common upper level, and the pump beam is tuned to the other.

In our case the pump beam tuned to one transition causes an increase in the common upper level that decays to the lower level of the other transition, increasing the population on this level. The second wave (diagnostic beam) is probed on this transition with an increase in the absorption. The effect occurs simultaneously for the two resonant rate groups with equal velocity but opposite direction. The crossover frequency is just halfway between the two hyperfine Lamb dips.

In this case the competition between optical pumping and collisional relaxation determines the size of the crossover dip. In the case of low pressure, optical pumping dominates and we have a negative crossover signal. In the case of high Ar pressure the collision process that produces relaxation from the lower filled state to the other lower level (the opposite velocity group) causes an increase of transmission, reducing the crossover signal. This result is shown in Fig. 5(b) for total reduction.

We obtained from the results of a least-squares fit of Eq. (12) the values for homogeneous broadening Γ , and

the relaxation velocity that is due to the VCC γ_{vc} of the ground state, as a function of the Ar pressure (Figs. 6 and 7, respectively). Our model is more accurate at low pressures. At higher pressures a more detailed treatment of the VCC is required.⁸

To obtain useful information we calculated the slope as the pressure tends to zero, as this is the case in which the collisional effects behave best. Thus from Fig. 6 we obtain

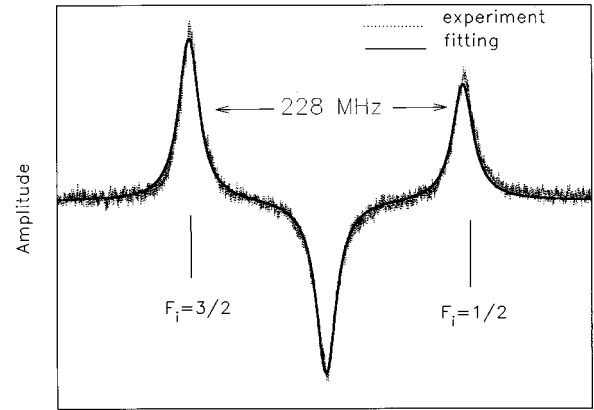
$$d\Gamma/dP = 2.5 \times 10^7 \text{ s}^{-1}/\text{Torr}. \quad (21)$$

Thus the collisional broadening FWHM is

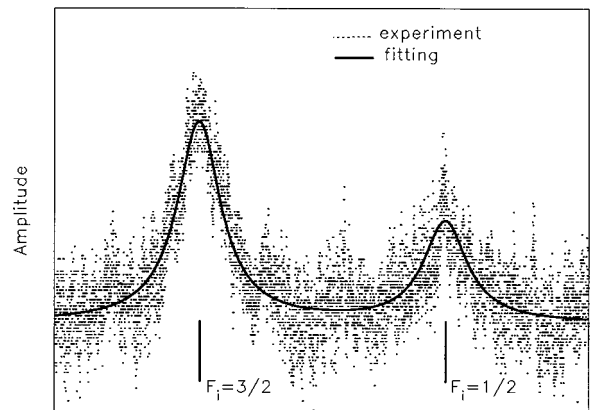
$$d(\Delta\nu)/dP = d\Gamma/dP/\pi = 8.0 \text{ MHz}/\text{Torr} \quad (22)$$

at our experimental conditions at 648 °K. Inasmuch as the collisional broadening is proportional to $T^{-7/10}$,²⁰ we rescale our results to 14 MHz/Torr at 300 °K. The value given in the literature is 12 MHz/Torr.²²

From Fig. 7, the change in the relaxation rate that is due to VCC by the Ar pressure is given by



(a)



(b)

Fig. 5. (a) Doppler-free spectrum at low Ar pressure: $P_{\text{Ar}} = 0.018 \text{ Torr}$, $I_p = 21 \text{ W/m}^2$, $n_{\text{Li}} = 5 \times 10^9 \text{ cm}^{-3}$, $T = 375 \text{ }^\circ\text{C}$. Result of the fitting: $\Gamma = 5.9 \times 10^7 \text{ s}^{-1}$, $\gamma_{vc} = 4.5 \times 10^6 \text{ s}^{-1}$. (b) Doppler-free spectrum at high Ar pressure. $P_{\text{Ar}} = 4.46 \text{ Torr}$, $I_p = 79 \text{ W/m}^2$, $n_{\text{Li}} = 5 \times 10^9 \text{ cm}^{-3}$, $T = 375 \text{ }^\circ\text{C}$. Result of the fitting: $\Gamma = 1.5 \times 10^8 \text{ s}^{-1}$, $\gamma_{vc} = 2.5 \times 10^7 \text{ s}^{-1}$.

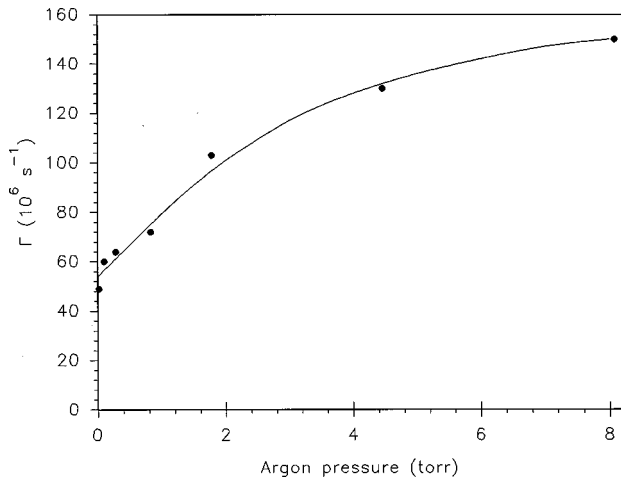


Fig. 6. Γ versus Ar pressure obtained from fitting of the Doppler-free spectra and extrapolating to $I_p = 0$.

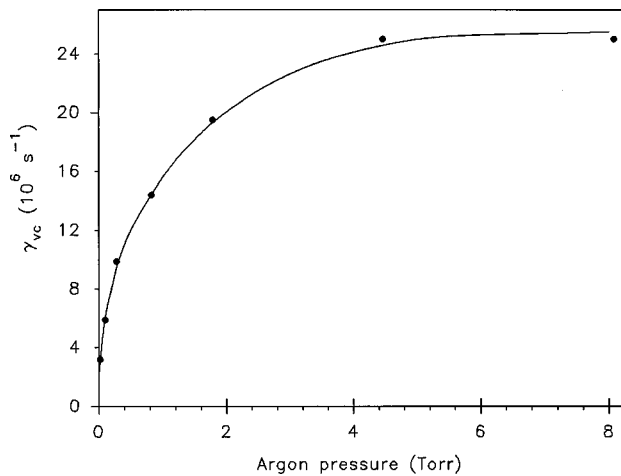


Fig. 7. γ_{vc} versus Ar pressure obtained from fitting of the Doppler-free spectra and extrapolating to $I_p = 0$.

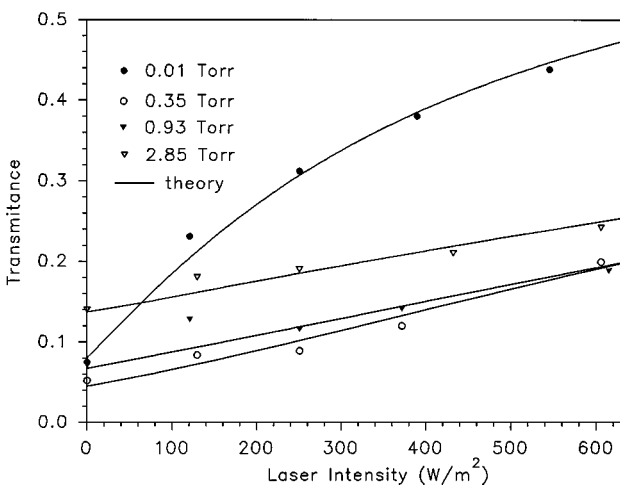


Fig. 8. Comparison of experimental and theoretical transmittance curves versus laser intensity (calculated starting from the Doppler-free spectra). $P = 0.01$ Torr: $\Gamma = 5.4 \times 10^7 \text{ s}^{-1}$, $\gamma_{vc} = 2.9 \times 10^6 \text{ s}^{-1}$. $P = 0.35$ Torr: $\Gamma = 6.3 \times 10^7 \text{ s}^{-1}$, $\gamma_{vc} = 1.0 \times 10^7 \text{ s}^{-1}$. $P = 0.93$ Torr: $\Gamma = 7.8 \times 10^7 \text{ s}^{-1}$, $\gamma_{vc} = 1.5 \times 10^7 \text{ s}^{-1}$. $P = 2.85$ Torr: $\Gamma = 1.1 \times 10^8 \text{ s}^{-1}$, $\gamma_{vc} = 2.2 \times 10^7 \text{ s}^{-1}$.

$$d\gamma_{vc}/dP = 3.2 \times 10^7 \text{ s}^{-1}/\text{Torr} = 3.3 \times 10^5 \text{ s}^{-1}/\text{Pa}. \tag{23}$$

We have that $\gamma_{vc} = \sigma_{vc} v_{rel} n$ and $v_{rel} = (8k_B T/\pi\mu)^{1/2}$, where $\mu = 8.66 \times 10^{-27} \text{ kg}$ is the reduced mass for the Li-Ar system. We obtained $\sigma_{vc} \approx 1.8 \times 10^{-14} \text{ cm}^2$, whose range from the literature⁸ is $1.01\text{--}2.4 \times 10^{-14} \text{ cm}^2$. For low Ar pressures Γ is given only by natural broadening, transit-time broadening, laser broadening, collisions between Li atoms, and less important relaxation mechanisms not considered here.

We obtained values for the transmittance at the center of the D_2 line for ^6Li starting from the Doppler-limited spectra discussed above; we show them in Fig. 8.

For each pressure we obtained the expected values for Γ and γ_{vc} by interpolating the curves in Figs. 6 and 7. With these values of Γ and γ_{vc} we calculated the transmittance versus intensity curve for each pressure starting from Eq. (10) in the steady state.

The value for nx can be obtained from the Doppler-limited absorption measurements described in Section 2. Figure 8 shows good agreement between theoretical and experimental curves; thus the technique to estimate Γ and γ_{vc} is shown to be satisfactory.

5. CONCLUSION

We have measured and resolved the hyperfine structure of the D_2 ^6Li line. We also investigated the relaxation processes and applied a numerical technique to study the effect of the vapor conditions on the Doppler-free absorption spectra. These conditions include density, alkali-vapor pressure, buffer-gas pressure, temperature, and diode-laser intensity. We found excellent agreement between a theoretical absorption expression derived by density matrix methods given in Eq. (12) and the experimental data of the Doppler-free lines.

The method described in this paper is fairly simple; however, the theoretical results depend on indirect calculations, which can be a source of uncertainty. The results reported here further demonstrate that state-of-the-art diode lasers are powerful experimental tools for a variety of high-resolution and high-sensitivity laser spectroscopy. We applied these results to derive parameters of spectroscopic interest, such as the line broadening and the relaxation rates that are due to collisions between isotopic species with Ar atoms.

ACKNOWLEDGMENTS

This study was supported by Fondo de Ciencia y Tecnología (FONDECYT 1950183) and Comisión Chilena de Energía Nuclear (CCHEN 391). T. Lokajczyk was supported by the Deutsche Forschungsgemeinschaft (DFG) through Sonderforschungsbereich (SFB 191), and Andreas Dinklage was partially supported by the DFG through SFB 198.

REFERENCES

1. A. Dinklage, T. Lokajczyk, H. J. Kunze, B. Schweer, and I. E. Olivares, "In situ density measurements for a thermal

- lithium beam employing diode lasers," *Rev. Sci. Instrum.* **69**, 321–322 (1998).
2. J. Brust, D. Veza, and K. Niemax, "Collisional excitation-transfer between lithium isotopes," *Z. Phys. D* **32**, 305–309 (1995).
 3. M. G. Boshier, D. Berkeland, E. A. Hinds, and V. Sandoghar, "External-cavity frequency-stabilization of visible and infrared semiconductor lasers for high resolution spectroscopy," *Opt. Commun.* **85**, 355–359 (1991).
 4. M. Weidemuller, C. Gabbanini, J. Hare, M. Gross, and S. Haroche, "A beam of laser-cooled lithium Rydberg atoms for precision microwave spectroscopy," *Opt. Commun.* **101**, 342–346 (1993).
 5. S. N. Atutov, E. Mariotti, M. Meucci, P. Bicchi, C. Marielli, and L. Moi, "A 670 nm external-cavity single mode diode laser continuously tunable over 18 GHz range," *Opt. Commun.* **107**, 83–87 (1994).
 6. J. Chen, J. G. Story, J. J. Tollet, and R. G. Hulet, "Adiabatic cooling of atoms by an intense standing wave," *Phys. Rev. Lett.* **69**, 1344–1346 (1992).
 7. C. J. Sansonetti, B. Richou, R. Engelman, Jr., and L. J. Radziemski, "Measurements of the resonance lines of ^6Li and ^7Li by Doppler-free frequency modulation spectroscopy," *Phys. Rev. A* **52**, 2682–2688 (1995).
 8. G. Shimkaveg, W. W. Quivers, Jr., R. R. Dasari, and M. S. Feld, "Direct measurement of velocity-changing collision cross section by laser optical pumping," *Phys. Rev. A* **48**, 1409–1418 (1993).
 9. C. Wieman and L. Hollberg, "Using diode lasers for atomic physics," *Rev. Sci. Instrum.* **62**, 1–20 (1991).
 10. J. Franzke, A. Schnell, and K. Niemax, "Spectroscopic properties of commercial laser diodes," *Spectrochim. Acta Rev.* **15**, 379–95 (1993).
 11. P. Zorabedian, "Tunable external-cavity semiconductor lasers," in *Tunable Lasers Handbook*, F. J. Duarte, ed. (Academic, New York, 1995), pp. 349–442.
 12. F. J. Duarte, "Dispersive external cavity semiconductor lasers," in *Tunable Laser Applications*, F. J. Duarte, ed. (Dekker, New York, 1995), pp. 153–178.
 13. W. Happer, "Optical pumping," *Rev. Mod. Phys.* **44**, 169–249 (1972).
 14. R. Loudon, "Quantum mechanics of the atom-radiation interaction," in *The Quantum Theory of Light*, 2nd ed., R. Loudon, ed. (Clarendon, Oxford, 1981), pp. 39–78.
 15. R. D. Cowan, ed., *The Theory of Atomic Structure Spectra* (U. California Press, Berkeley, Calif., 1981).
 16. H. J. Andra, "Precision experiments using fast beam laser interaction," *Nucl. Instrum. Methods* **202**, 123–137 (1982).
 17. E. Arimondo, M. Inguscio, and P. Violino, "Experimental determinations of the hyperfine structure in the alkali atoms," *Rev. Mod. Phys.* **49**, 31–75 (1977).
 18. J. R. Ackerhalt and B. W. Shore, "Rate equations versus Bloch equations in multiphoton ionization," *Phys. Rev. A* **16**, 277–282 (1977).
 19. M. G. Payne, L. Deng, and N. Thonnard, "Applications of resonance ionization mass spectrometry," *Rev. Sci. Instrum.* **65**, 2433–2459 (1994).
 20. G. S. Hurst, M. G. Payne, S. D. Kramer, and J. P. Young, "Resonance ionization spectroscopy and one atom detection," *Rev. Mod. Phys.* **51**, 767–819 (1979).
 21. P. G. Pappas, M. M. Burns, D. D. Hinshelwood, M. S. Feld, and D. E. Murnik, "Saturation spectroscopy with optical pumping in atomic barium," *Phys. Rev. A* **21**, 1955–1968 (1980).
 22. W. Demtröder, *Laser Spectroscopy Basic Concepts and Instrumentation* (Springer-Verlag, Berlin, 1993).
 23. K. E. Gibble and A. Gallagher, "Measurements of velocity-changing collision kernels," *Phys. Rev. A* **43**, 1366–1380 (1991).
 24. R. M. Herman, "Noble-gas-induced rubidium spin disorientation," *Phys. Rev. A* **136**, 1576–1582 (1964).
 25. T. Holstein, "Imprisonment of resonance radiation in gases," *Phys. Rev.* **72**, 1212–1233 (1947).
 26. D. W. Marquardt, "An algorithm for least-squares estimation of nonlinear parameters," *J. Soc. Ind. Appl. Math.* **11**, 431–435 (1963).
 27. C. R. Vidal, "Spectroscopic observations of subsonic and sonic vapor inside an open-ended heat pipe," *J. Appl. Phys.* **44**, 2225–2232 (1973).
 28. C. R. Vidal and J. Cooper, "Heat-pipe oven: a new, well-defined metal vapor device for spectroscopic measurements," *J. Appl. Phys.* **40**, 3370–3374 (1969).
 29. D. R. Lide, ed., *Handbook of Chemistry and Physics*, 71st ed. (CRC, Boca Raton, Fla., 1991), pp. 5–70.